

Three-dimensional instability of the flow around a rotating circular cylinder

Jan O. Pralits^{1,†}, Flavio Giannetti² and Luca Brandt³

¹DICCA, University of Genoa, Via Montallegro 1, 16145 Genoa (GE), Italy

²DIIN, University of Salerno, Via Ponte don Melillo, 84084 Fisciano (SA), Italy

³Linné Flow Centre, KTH Mechanics, S-100 44 Stockholm, Sweden

(Received 17 January 2013; revised 10 June 2013; accepted 22 June 2013;
first published online 30 July 2013)

The two-dimensional stationary flow past a rotating cylinder is investigated for both two- and three-dimensional perturbations. The instability mechanisms are analysed using linear stability analysis and the complete neutral curve is presented. It is shown that the first bifurcation in the case of the rotating cylinder occurs for stationary three-dimensional perturbations, confirming recent experiments. Interestingly, the critical Reynolds number at high rotation rates is lower than that for the stationary circular cylinder. The spatial characteristics of the disturbance and a qualitative comparison with the results obtained for linear flows suggest that the stationary unstable three-dimensional mode could be of hyperbolic nature.

Key words: vortex streets, wakes/jets

1. Introduction

The flow past a circular cylinder often serves as a prototype to investigate the vortex formation and wake dynamics behind bluff bodies. In the case of a stationary cylinder the different bifurcations occurring when increasing the Reynolds number are well known. Here the Reynolds number is based on the dimensional free-stream velocity U_∞^* , the cylinder diameter D^* and the kinematic viscosity ν^* . The steady two-dimensional symmetric flow becomes unstable above a critical value $Re \approx 47$ (see Provansal, Mathis & Boyer 1987) via a Hopf bifurcation (see Noack & Eckelmann 1994) giving rise to a self-sustained structure usually termed Kármán vortex street. For values of Re above ≈ 190 the flow becomes unstable to three-dimensional perturbations, (see, e.g., Barkley & Henderson 1996; Williamson 1996). The rotating cylinder and corresponding bifurcations, on the other hand, have been studied primarily in the two-dimensional framework (see Kang, Choi & Lee 1999; Stojković, Breuer & Durst 2002; Mittal & Kumar 2003; Stojković *et al.* 2003; Pralits, Brandt & Giannetti 2010). A complete neutral curve for two-dimensional perturbations as a function of the rotation rate α and the Reynolds number is found in both Stojković *et al.* (2003) and Pralits *et al.* (2010). The rotation rate is here defined as $\alpha = \Omega D^*/(2U_\infty^*)$ with Ω representing the cylinder angular velocity. In both investigations two different types of disturbances can be distinguished. The so-called mode I is similar (equal when $\alpha = 0$) to the classical von Kármán instability. Unstable

† Email address for correspondence: jan.pralits@unige.it

solutions are found for $Re > 47$ and low rotation rates. As the Reynolds number is increased the neutral curve of mode I is found for $\alpha(Re) \rightarrow 2$. At higher rotation rates a second instability, denoted mode II, exists and has a frequency one order of magnitude lower than that of mode I. For a given Re it persists for a narrow range of rotation rates and the critical Reynolds number is slightly below the value of 50. In the vicinity of the upper neutral branch of mode II multiple stationary solutions were found for a fixed Reynolds number (see Pralits *et al.* 2010). These solutions were computed using arclength continuation and two turning points were found. Pralits *et al.* (2010) also presented the bifurcation diagram of two-dimensional instabilities for the multiple solutions. In particular, it was shown that the second turning point determines the rotation rate at which an unstable solution is last observed. In fact, this point defines the birth of a branch with stable steady-state solutions that continues at larger α .

Pralits *et al.* (2010) conducted a structural sensitivity analysis using a combination of direct and adjoint global modes in order to provide relevant knowledge about the origin of the instability. In particular, the core region for the instability mechanism and the sensitivity to steady variations of the underlying base flow were identified. The structural sensitivity of mode II has its maximum close to the stagnation point while the sensitivity with respect to the base flow was shown to have its maximum in the low-rear part of the cylinder, in a region opposite to the stagnation point.

Experimental measurements of the flow past a rotating cylinder were performed by Barnes (2000) at low rotation rates to determine the value at which shedding is suppressed for Reynolds numbers between 50 and 65. The findings agrees with the results of, e.g., Kang *et al.* (1999), Stojković *et al.* (2002) and Pralits *et al.* (2010) who showed that the vortex shedding behind a rotating cylinder disappears when α is increased above the value of 2. To the best of the authors' knowledge only the experimental work by Yildirim *et al.* (2008) reports a low-frequency shedding at $Re = 100$ and $\alpha = 5.1$. In an initial transient phase they observed a tilted vortex structure in the wake of the cylinder and the measured frequency was similar to the computations by, e.g., Stojković *et al.* (2003) and Pralits *et al.* (2010). However, the vorticity core was located on the opposite side of the wake and their experiment cannot be considered a verification of the existence of mode II.

To the best of the authors' knowledge, only few works have been concerned with the three-dimensional stability characteristics of the rotating cylinder flow. The investigation by ElAkoury *et al.* (2008) indicates that the cylinder rotation has a stabilizing effect on three-dimensional perturbations thus increasing the Reynolds number for two-dimensional/three-dimensional transition to values larger than that observed for the flow past a non-rotating cylinder. In the recent work by Rao *et al.* (2013) a detailed study regarding the transition from steady to unsteady flow is made along with a mapping of the transition from two-dimensional to three-dimensional flow. It is shown that vortex shedding is suppressed for $\alpha \geq 2.1$ for all Reynolds numbers and that transition to three-dimensional flow occurs for Reynolds number slightly below the value of 200. However, these authors did not investigate values of the rotation rate above 2.5.

It is known that when further increasing the rotation speed, the stagnation point moves away from the surface of the cylinder, and closed streamlines form, separating the flow internal and external to it. Within the internal flow, one can expect large pressure differences and Mittal (2004), who investigated the flow at $\alpha = 5$ and $Re = 200$, argued that this will cause the appearance of three-dimensional centrifugal instabilities, with spanwise scale $\lambda \approx D$.

Further investigations are needed on the onset of a three-dimensional flow past a rotating circular cylinder. In this work we therefore investigate the stability characteristics of three-dimensional perturbations superimposed on the stationary two-dimensional base flow using global stability analysis. Neutral curves, critical rotation rates and critical Reynolds numbers are presented in order to determine the onset of three-dimensional instabilities. The results are compared with the recent results in the Doctoral thesis by Linh (2011) where experiments of the flow past a rotating cylinder are presented, and a possible explanation is given for the difficulties of previous experimental investigations (e.g. Yildirim *et al.* 2008) in detecting the low-frequency vortex shedding at high rotation rates, the so-called mode II. A structural sensitivity analysis is also conducted with the purpose of establishing the region responsible for the generation of the instability. Finally, an indication regarding where to position a passive control device is shown based on a structural sensitivity analysis with respect to base-flow modifications.

In the following we will denote modes at rotation rates $\alpha < 2$ as mode I and modes for higher rotation rates, $\alpha > 2$, as mode II. This is to be consistent with earlier investigations in which a similar notation has been used.

2. Linear stability analysis and numerical method

The instability onset is studied using linear theory and a normal-mode analysis. The flow quantities are decomposed in a steady part and a small unsteady perturbation as

$$\mathbf{U}(x, y, t) = \mathbf{U}_b(x, y) + \epsilon \frac{1}{\sqrt{2\pi}} \int_{-\infty}^{\infty} \mathbf{u}(x, y, \kappa, t) \exp(i\kappa z) d\kappa, \tag{2.1}$$

where the amplitude ϵ is assumed to be small and a Fourier transform is used to express the spanwise dependence of a general three-dimensional perturbation. The same decomposition is used for the pressure. The base flow $\mathbf{U}_b(x, y)$ satisfies the steady Navier–Stokes equations for two-dimensional incompressible flow at a given Reynolds number Re and rotation rate α . The rotation of the cylinder is imposed as a boundary condition such that $\mathbf{U}_b \cdot \mathbf{t} = \alpha$ and $\mathbf{U}_b \cdot \mathbf{n} = 0$. Here \mathbf{t} and \mathbf{n} are the tangential and normal versors to the cylinder surface. The dimensional free-stream velocity U_∞^* and diameter D^* are used as reference velocity and length scales throughout the paper. Three-dimensional global modes are analysed assuming $\mathbf{u}(x, y, \kappa, t) = \hat{\mathbf{u}}(x, y, \kappa) \exp(\sigma t)$ and $p(x, y, \kappa, t) = \hat{p}(x, y, \kappa) \exp(\sigma t)$. Introducing this decomposition into the Navier–Stokes equations and collecting terms of order ϵ we obtain the linearized unsteady Navier–Stokes equations

$$\sigma \hat{\mathbf{u}} + \mathbf{L}_\kappa \{ \mathbf{U}_b, Re \} \hat{\mathbf{u}} + \nabla_\kappa \hat{p} = \mathbf{0}, \tag{2.2}$$

$$\nabla_\kappa \cdot \hat{\mathbf{u}} = 0. \tag{2.3}$$

In the above expression $\nabla_\kappa \equiv (\partial_x, \partial_y, i\kappa)$ is the modified gradient operator and \mathbf{L}_κ denotes the modified three-dimensional linearized Navier–Stokes operator. On the cylinder surface a no-slip boundary condition is imposed while in the far field appropriate radiative boundary conditions are used. For further details and notation see Giannetti & Luchini (2007). The system (2.2)–(2.3) gives rise to a generalized eigenvalue problem for the complex eigenvalue σ . For $\text{Re}(\sigma) < 0$ the flow is stable while for $\text{Re}(\sigma) > 0$ the mode is unstable and grows exponentially in time.

2.1. Numerical method

The results presented here are obtained with the numerical code described in Giannetti & Luchini (2007). A second-order finite-difference approach is used to compute spatial derivatives of the governing partial differential equations together with an immersed-boundary technique to represent the cylinder surface on a Cartesian mesh. The computational domain is rectangular. The steady nonlinear Navier–Stokes equations are solved by Newton iteration in order to compute the base flow used for the linear stability analysis. Arc-length continuation is adopted for rotation rates above the onset of the second mode where multiple steady state solutions exist. Further, the stability of the flow is investigated through the eigenvalue problem defined by the linearized perturbation equations (2.2)–(2.3), where an implicitly restarted Arnoldi algorithm is implemented to compute the least stable eigenvalue and eigenmode. The main results are obtained with a computational domain of length $L_x = 50$, $L_y = 30$ in the streamwise x - and cross-stream y -direction, respectively. The cylinder is located symmetrically between the upper and lower boundaries, 15 diameters downstream of the inflow. The Cartesian coordinate system has its origin in the centre of the cylinder ($x_c = 0$, $y_c = 0$). The computational mesh is non-uniform, see e.g. Giannetti & Luchini (2007), with a resolution of 400×300 points in the x and y directions, respectively. A square domain measuring 2×2 diameters, with its centre coinciding with that of the cylinder, has a uniform mesh containing 100 grid points in each direction. The results have been validated by varying both resolution and domain size.

3. Stability characteristics

The onset of three-dimensional instabilities is investigated by solving the linear stability problem outlined in §2 for different values of the Reynolds number, rotation rate and spanwise wavenumber. The growth rate σ_r and Strouhal number $St = \sigma_i/(2\pi)$ of the least stable modes pertaining to the stationary base flows at $Re = 100$ and two different rotation rates $\alpha = 4.75$ and 5 are presented in figure 1 as a function of the spanwise wavenumber κ . In particular we focus on the two least stable modes and the reason will be discussed in this section.

When the spanwise wavenumber is small, the perturbation Strouhal number is non-zero and the corresponding maximum growth rate is found for $\kappa = 0$, the so-called unsteady mode II. For increasing values of the spanwise wavenumber the least stable solution is stationary. This is a novelty compared with previous investigations conducted in a two-dimensional framework. At $\alpha = 5$ the maximum growth rate of the stationary mode is about three times that of the unsteady mode. Moreover, the unstable stationary perturbation remains unstable for values of α where the unsteady one is already stable (here $\alpha = 4.75$). Finally, for intermediate values of κ there exists a range of values of α where the unsteady and stationary modes are unstable simultaneously (here $\alpha = 5$ and $\kappa \approx 0.3$). The results presented in figure 1 are exploited more in detail in figure 2 where the growth rate ($\sigma_r \geq 0$) of the least stable mode is presented as a function of α and κ at four different values of the Reynolds number. One can first of all note that in all figures that the mode $\alpha = 0$, $\kappa = 0$ is the classical von Kármán instability (appearing when $Re > 47$). Shedding mode I is reported for $Re = 50, 60, 100$ when $\alpha < 2$. For this unsteady instability the largest growth rate is always obtained for $\kappa = 0$. Further, the range of κ for which unstable solutions exist increases with increasing Reynolds number. The corresponding frequencies of mode I are similar to the values obtained when $\kappa = 0$ as shown by, e.g., Pralits *et al.* (2010).

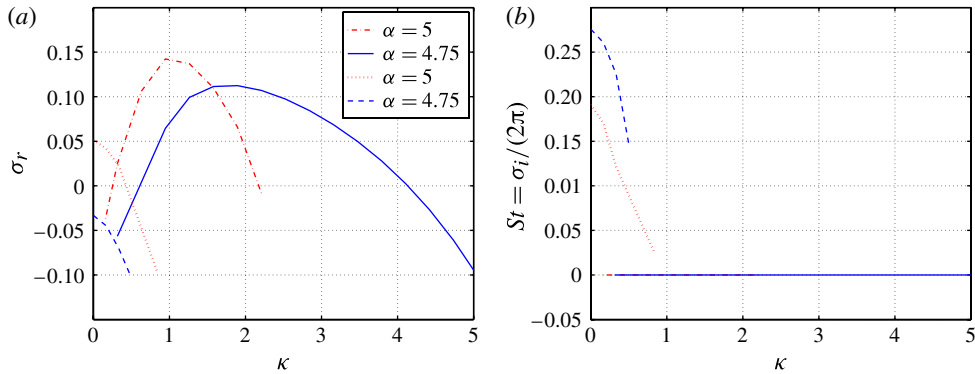


FIGURE 1. (Colour online) Growth rate σ_r (a) and Strouhal number $St = \sigma_i / (2\pi)$ (b) for $Re = 100$ as a function of the rotation rate α and spanwise wavenumber κ . The stationary modes are indicated by the solid lines while the unsteady modes by the dashed lines.

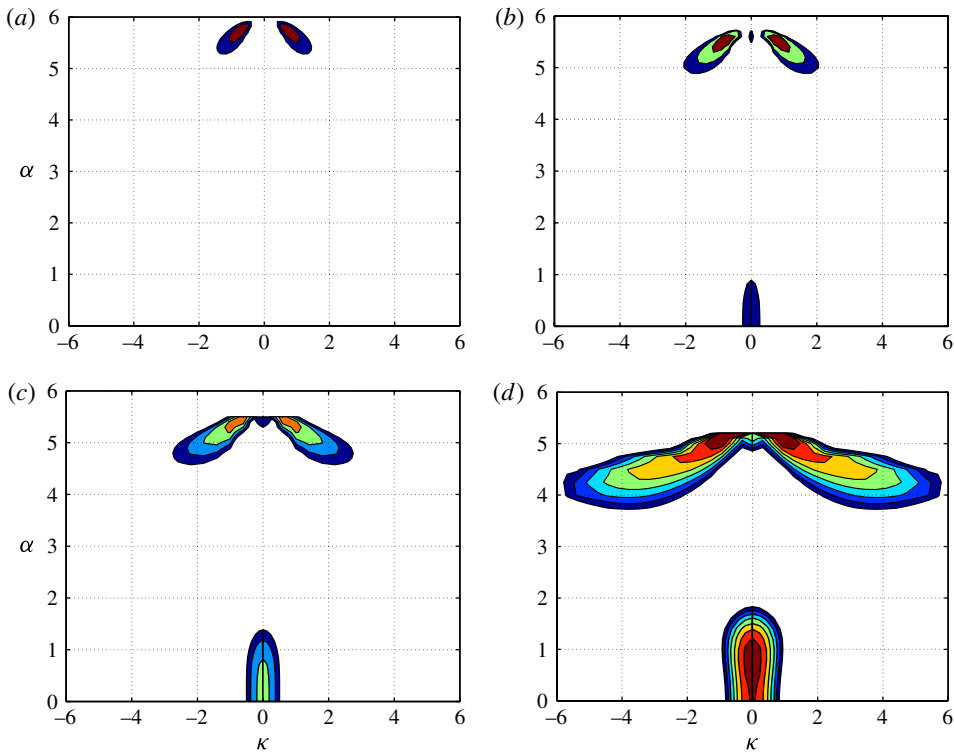


FIGURE 2. (Colour online) Growth rate $\sigma_r \geq 0$ in the plane (α, κ) : (a) $Re = 40$; (b) $Re = 50$; (c) $Re = 60$; and (d) $Re = 100$. The contour spacing is 0.02 in all figures.

For higher rotation rates, roughly between 3 and 6, unstable solutions are found for all Reynolds numbers presented but we have to make a distinction between what we will denote unsteady mode II and stationary mode II. The unsteady mode II is characterized by small values of κ and it is essentially the same mode presented by,

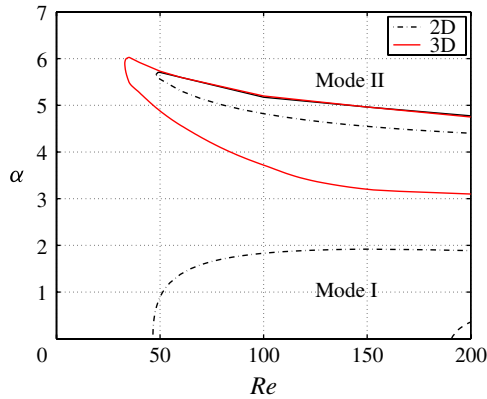


FIGURE 3. (Colour online) Neutral stability curve ($\text{Re}(\sigma) = 0$) in the Re - α plane showing the regions delimited by mode I and II, respectively. The curve denoted by 3D is the upper and lower branch over all spanwise wavenumbers (κ). The curve denoted 2D is the neutral curve for two-dimensional ($\kappa = 0$) modes Pralits *et al.* (see, e.g., 2010). The dashed curve in the vicinity of $Re = 200$, $\alpha = 0$ is taken from Rao *et al.* (2013) and represents the bifurcation to three-dimensional instabilities.

e.g., Pralits *et al.* (2010) and Stojković *et al.* (2003). The maximum growth rate is found for $\kappa = 0$ and the critical Reynolds number is just below the value of 50.

The stationary mode II on the other hand, reaches the largest growth rate for spanwise wavenumbers from ~ 0.5 to 6 and rotation rates roughly between 3 and 6, depending on the Reynolds number. For relatively large Reynolds numbers, $Re = 100$, the rotation rate ranges between 3.7 and 5.3 while the wavenumber ranges between 0.5 and 6. As the Reynolds number is decreased both the range in rotation rate and spanwise wavenumber decrease. It is interesting to note that the stationary mode II is still unstable for Reynolds numbers below the value of 47. The first bifurcation for the flow around a rotating cylinder, when $\alpha > 2$, is therefore to a stationary three-dimensional flow.

A summary of the stability analysis is presented in figure 3 by the neutral curve ($\sigma_r = 0$) as a function of the Reynolds number and the rotation rate. The results for $\alpha < 2$ are in agreement with the numerical results by Pralits *et al.* (2010) and Stojković *et al.* (2003) since the most amplified mode I is two-dimensional. The neutral curve for $\alpha > 2$ is given by the minimum and maximum values of α for which neutral solutions are found, as a function of the spanwise wavenumber, at each Reynolds number. This curve is denoted by 3D in the figure. For completeness we report also the neutral curve for two-dimensional mode II as was presented by Pralits *et al.* (2010). It is shown that the range of α corresponding to three-dimensional perturbations is 2–3 times larger than that obtained for two-dimensional perturbations at each Re . Note that a neutral curve taking into account only three-dimensional unsteady perturbations would be contained within the neutral curve denoted by 2D. This can be understood by looking at figure 2 which shows the growth rate $\sigma_r \geq 0$. The critical values of Re and α in figure 3 are 33 and 5.8, respectively.

4. Comparison with experiments

In this section results from the linear stability analysis are compared with the recent experimental measurements by Linh (2011). This author performed an experimental

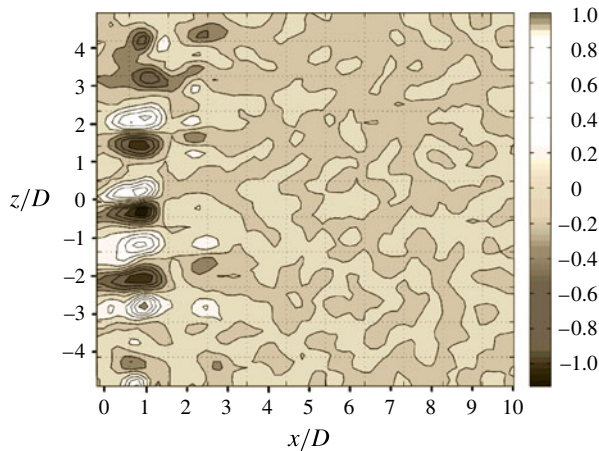


FIGURE 4. (Colour online) Experiments by Linh (2011) for $Re = 206$ showing the spanwise vorticity in the x - z plane at a distance $0.56D$ in the y direction on the side of the stagnation point. From these data Linh (2011) estimated the spanwise wavelength of the three-dimensional structures to be between $\lambda \approx 1D$ – $1.5D$. The corresponding spanwise wavenumbers are $\kappa = 2\pi/\lambda \approx 6.3$ – 4.2 .

investigation of the flow past a rotating cylinder in a closed loop channel. The turbulence intensity was $\sim 1\%$, and the cylinder length to diameter ratio was 25 for $Re < 500$. The latter ensures that the flow remains strictly two-dimensional for low Reynolds numbers. Dye and particle tracing flow visualization (PTFV) were used to visualize the flow while a hot-film anemometer and particle image velocimetry (PIV) were employed to obtain flow field measurements. In particular, a Litron laser system and a Dantec PIV2100 processor system were used for the PIV where the flow was seeded with glass particles which had a diameter of $10\ \mu\text{m}$. Measurements were made in both the streamwise (x - y) plane and the spanwise (x - z) plane for $Re = 206, 334, 541, 1067$ with α ranging from 0 to 5. No evidence of the unsteady mode II earlier shown in numerical investigations by, e.g., Stojković *et al.* (2003) and Pralits *et al.* (2010) could be found in the experiments.

A periodic stationary pattern was instead observed in the spanwise plane for certain values of the rotation rate. The spanwise distribution of vorticity from the PIV measurements, which has its axis in the y direction, is shown in figure 4 for $Re = 206$ and $\alpha = 4$. Here the x - z plane is situated $0.56D$ away from the cylinder centre in the y direction on the side of the stagnation point. From this image we can estimate the spanwise wavelength of the three-dimensional modes to be between $\lambda \approx 1D$ – $1.5D$ (values reported in the thesis). These values correspond to spanwise wavenumbers $\kappa = 2\pi/\lambda \approx 6.3$ – 4.2 . In order to compare with the experimental results we performed a linear stability analysis for the same parameters (Re, α, κ) and determined the least-stable modes. Their growth rate is presented in figure 5 as a function of the spanwise wavenumber. The linear stability analysis gives the maximum growth rate for the spanwise wavenumber $\kappa \approx 6$ which is within the range of κ 's evaluated from the measurements by Linh (2011), here indicated by the grey area in the figure. Spanwise structures, similar to those presented in figure 4, were also found in the experiment by Linh for $Re = 206$ and $\alpha = 3$, but not for $\alpha = 1, 2, 5$. This is also consistent with the neutral stability curve presented in figure 3. The comparison shows that the linear

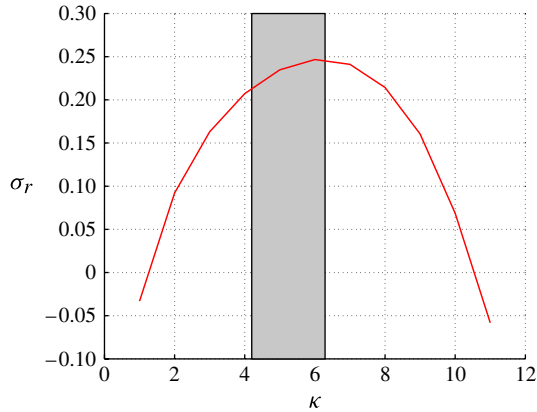


FIGURE 5. (Colour online) Growth rate σ_r obtained from the linear stability analysis as a function of κ at $Re = 206$. The values of κ corresponding to the wavelength's obtained from figure 4 are given by the grey area.

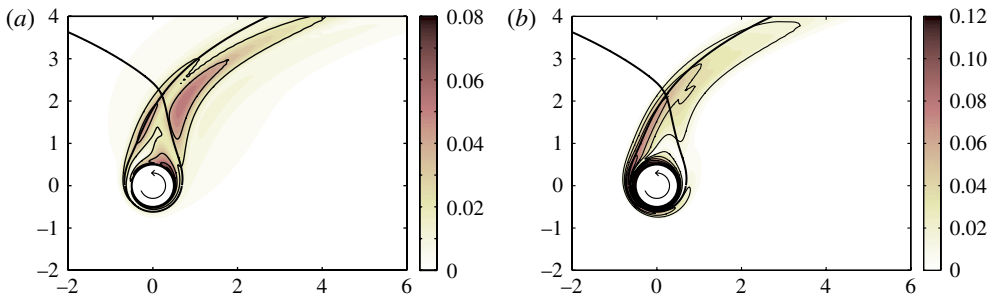


FIGURE 6. (Colour online) Modulus of the perturbation vorticity $|\omega(x, y)|$ at $Re = 100$ and $\alpha = 5$; $\kappa = 0$ (a) and $\kappa = 1$ (b). The black curve shows the streamlines passing through the stagnation point. The contour spacing is 0.02.

stability analysis performed here captures the main characteristics of the wake at high rotation rates and strengthens the results presented in figure 3.

5. The global modes

In this section we visualize the spatial structure of the modes corresponding to the unstable solutions shown in the previous section. In figure 6 the modulus of the vorticity field of mode II is presented for the case in which $Re = 100$ and $\alpha = 5$. The three-dimensional stationary mode II, with $\kappa = 1$, is compared with the unsteady two-dimensional counterpart ($\kappa = 0$). Both modes are unstable and the wavenumber for the stationary mode was chosen to maximize the growth rate (cf. figure 1). At this Reynolds number and rotation rate the streamlines crossing the stagnation point forms a closed loop around the cylinder. The spatial structures of the unsteady and stationary unstable modes are similar but the stationary mode has the maximum value of the vorticity modulus aligned with the direction of maximum strain of the base flow. Implications of this alignment is discussed later in this section. Figure 7 shows the spatial structure of the perturbation velocity for the stationary

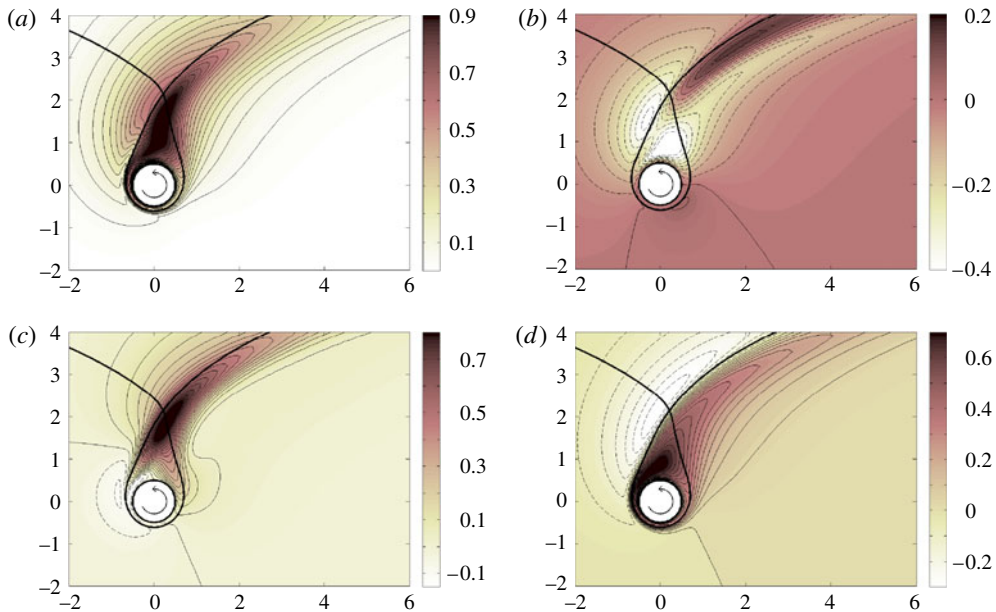


FIGURE 7. (Colour online) Spatial structure of the perturbation velocity at $Re = 100$, $\alpha = 5$ and $\kappa = 1$: (a) modulus; (b) horizontal component u ; (c) vertical component v ; (d) spanwise component w . The mode has been normalized such that the maximum of the modulus is 1. The contour spacing is 0.05 and continuous lines are positive values while dashed lines are negative values.

mode II at $Re = 100$, $\alpha = 5$ and $\kappa = 1$. Here both the modulus and the three velocity components are displayed: as can be easily noticed the mode grows in the region around the hyperbolic point, mainly inside the closed loop delimited by the streamlines crossing the stagnation point. A deeper knowledge of the instability characteristics can be gained using the concept of a wave-maker that is related to the region in space where a modification in the structure of the problem produces the largest drift of the eigenvalue. This is done by determining the region where feedback from velocity to force is most effective. This concept was introduced for the first time in Giannetti & Luchini (2007) in the context of a linear stability analysis on a steady base flow and later generalized in Luchini, Giannetti & Pralits (2008) to time-periodic flows. The sensitivity tensor \mathbf{S}_p derived by Giannetti & Luchini (2007) is given by

$$\mathbf{S}_p(x_0, y_0, \kappa) = \frac{\hat{\mathbf{u}}^*(x_0, y_0, \kappa) \hat{\mathbf{u}}(x_0, y_0, \kappa)}{\int_{\mathcal{D}} \hat{\mathbf{u}}^* \cdot \hat{\mathbf{u}} \, dS}, \quad (5.1)$$

where $\hat{\mathbf{u}}^*$ is the adjoint perturbation velocity, and $\hat{\mathbf{u}}^* \hat{\mathbf{u}}$ indicates the dyadic product between the direct and adjoint modes. Different norms of the tensor \mathbf{S}_p can be used to build a spatial map of the sensitivity. In figure 8 the spectral norm of the sensitivity tensor \mathbf{S}_p is presented for the same parameters used in figure 6. The maximum value is found in the vicinity of the stagnation point both for unsteady and stationary mode II, moreover, aligned with the direction of compression. The sensitivity of the stationary mode, however, is smaller in magnitude and its spatial structure presents a second

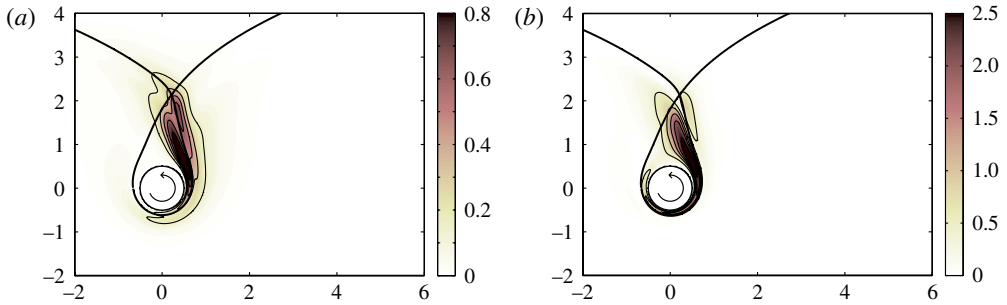


FIGURE 8. (Colour online) Structural sensitivity \mathcal{S}_p for $Re = 100$, $\alpha = 5$: (a) $\kappa = 0$; (b) $\kappa = 1$. The contour spacing is (a) 0.16, (b) 0.5.

peak in a region very close to the hyperbolic stagnation point. This fact suggests some considerations on the nature of the stationary mode II.

It is well known that in an inertial frame any inviscid incompressible flow with a stagnation point is unstable to short wavelength perturbations, no matter which type of flow surrounds it (see Friedlander & Vishik 1991; Lifschitz & Hameiri 1991). Various growth mechanisms have been presented to explain the development of such instabilities, depending on the elliptic or hyperbolic nature of the stagnation point. In the hyperbolic case the instability can be understood physically in terms of the stretching of the vorticity perturbations and the tilting of the velocity by the two-dimensional background flow. Such mechanism is an example of the so-called ‘Orr mechanism’ and leads transiently to elevated growth. Asymptotically this inviscid mechanism leads to exponentially growing modes with a velocity vector which aligns with the principal direction of compression of the base flow while the vorticity ultimately approaches a direction perpendicular to it (see Leblanc & Godeferd 1999; Caulfield & Kerswell 2000).

For idealized flows such as those characterized by a quadratic streamfunction, in fact, the maximum growth rate is attained by the so-called ‘pressureless modes’ which have a velocity perturbation that is purely two-dimensional ($w = 0$). Moreover, provided that the magnitude of the spanwise wavenumber is sufficiently large, the perturbation is predicted to grow even in a viscous flow, since the stabilizing effect of the fluid viscosity is dominated by the growth of the perturbation. As already noted, the flow around the rotating cylinder is characterized by the existence of a hyperbolic stagnation point whose position depends on the values of the Reynolds number Re and of the rotation rate α . In its proximity, the velocity perturbation vector is aligned with the direction of compression and has a spanwise component significantly smaller than the streamwise and vertical components. This can be clearly seen in figure 9(a) in which three different lines are drawn. The white one is the streamline of the base flow passing through the stagnation point, while the other two are obtained by integration of the differential equations $dx/dt = f(x)$ where the vector field f is taken to be the mode velocity (black line) and the mode vorticity (dashed line). The computations are performed in three dimensions, both forward and backward in time, with the initial seeds taken along the stagnation line. Since the corresponding global mode is stationary, these lines are parallel in each point to the corresponding vector fields used to generate them. The black lines in particular are therefore the streamlines of the unstable mode and can be used to better visualize its spatial structure in proximity to

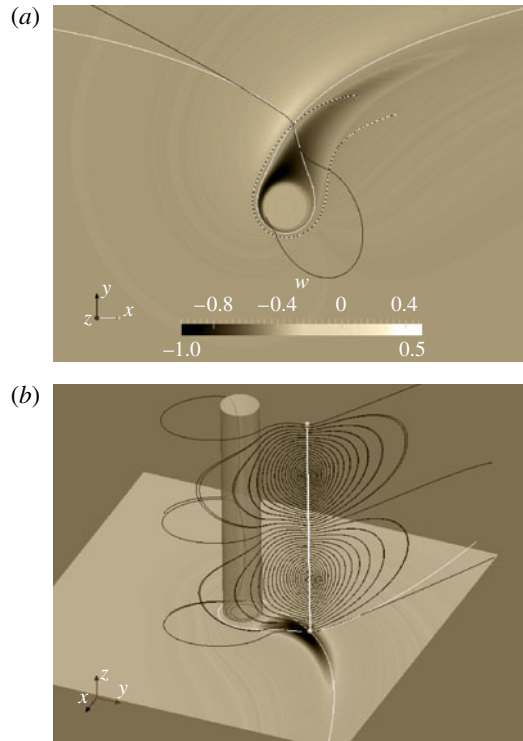


FIGURE 9. (Colour online) (a) Streamlines at $Re = 100$, $\alpha = 5$, $\kappa = 1$, passing through the hyperbolic point; base flow (white); mode (black). The dashed curve passes the stagnation point parallel to the perturbation vorticity. The colour map shows the spanwise component in an x - y plane where it reaches its maximum. The mode is normalized such that $\|\mathbf{u}\| = 1$. (b) Three-dimensional view of the mode streamlines passing through the stagnation line. The colour map represents the modulus of the perturbation velocity in a plane where the spanwise component vanishes. The white line is the streamline of the base flow passing through the hyperbolic point.

the hyperbolic point. The colour map in the background corresponds to the spanwise component of the perturbation velocity on a plane where it reaches its maximum.

Figure 9(b) shows a three-dimensional view of the mode streamlines passing through the stagnation point and shows that in its proximity the perturbation velocity is contained in the plane tangent to the stagnation line (in white). The colour map at the base of the figure shows the modulus of the perturbation velocity in a plane where the w component vanishes. Note that the mode maximum is located close to the hyperbolic point. Thus, at least locally, there is a qualitative resemblance with the ‘pressureless’ perturbations described by Leblanc & Godefert (1999) and Caulfield & Kerswell (2000). Note also that for the rotating cylinder the maximum growth rate is reached for values of the wavenumber $\kappa = O(1)$: this fact prevents us from a more quantitative comparison with the asymptotic theory, which is only valid in the large wavenumber limit. Furthermore, as we move away from the stagnation point, the flow quickly differs from a linear flow, so that the final growth rate is certainly influenced by the non-local characteristics of the base flow. This is also confirmed by the structural sensitivity analysis (figure 8) which shows that the instability mechanism

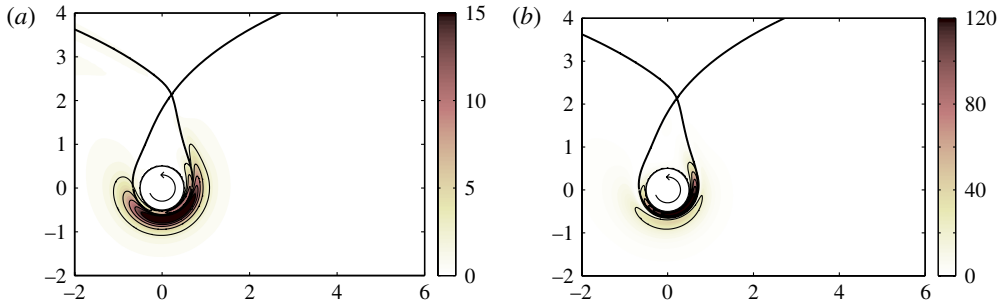


FIGURE 10. (Colour online) Structural sensitivity \mathbf{S}_b for $Re = 100$, $\alpha = 5$: (a) $\kappa = 0$; (b) $\kappa = 1$. The black curve shows the streamlines passing through the stagnation point. The contour spacing is (a) 3, (b) 24.

is localized inside the area delimited by the streamline passing through the stagnation point, in a region close to the hyperbolic point, but not exactly centred on it.

In theory, it is possible that other instability mechanisms act and cooperate to generate the unstable mode. For example, the region of the flow delimited externally by the stagnation streamline and internally by the cylinder is characterized by the presence of closed streamlines and can be prone to a centrifugal instability. This inviscid mechanism is due to the disruption of the balance between the centrifugal force and the radial pressure gradient and usually gives rise to modes which are localized along particular streamlines, with a transverse spatial structure which generally decays exponentially fast. Although viscosity and small wavenumbers effects can modify the structure of these modes considerably, the distinguishing characteristics of a centrifugal instability are not visible in the results presented in this study, at least in the range of parameters investigated. Thus, even if a more detailed investigation (which is outside the scope of this paper) is necessary to clarify the nature of the stationary instability, the main characteristics of the mode and the sensitivity analysis presented here strongly suggest that the stationary mode II is of hyperbolic nature.

In this last part we show the sensitivity tensor \mathbf{S}_b due to base flow modifications. The importance of analysing this quantity was discussed in detail in the work by Pralits *et al.* (2010) and is related to modifications of the basic flow induced by small objects such as e.g. a control cylinder whose purpose is to act as a passive control device. The expression of the sensitivity tensor can be written

$$\mathbf{S}_b(x_0, y_0, \kappa) = \frac{\mathbf{U}_b^*(x_0, y_0) \mathbf{U}_b(x_0, y_0)}{\int_{\mathcal{D}} \hat{\mathbf{u}}^* \cdot \hat{\mathbf{u}} \, dS}, \quad (5.2)$$

where \mathbf{U}_b^* is the solution of the adjoint base flow equations (see Pralits *et al.* 2010, for a complete derivation). In figure 10 the spectral norm is shown for the same parameters used in figures 6 and 8. The maximum sensitivity of the stationary three-dimensional mode II is approximately ten times that of the unsteady two-dimensional mode II. Further, the largest sensitivity of the stationary mode is located inside the closed streamlines on the lee-ward side of the stagnation point, while the unsteady mode has its maximum outside the closed streamlines. The results imply that different regions in space are important when it concerns control of the wake flow.

6. Conclusions

In this paper we have presented a linear stability analysis of the flow past a rotating cylinder and investigate the onset two-dimensional and three-dimensional bifurcations. We find a reasonable explanation for the discrepancies between numerical and experimental findings existing so far at large rotation rates. In this regime, all conditions being equal, if an unstable two-dimensional unsteady solution exists then a three-dimensional stationary unstable solution also exists but with a larger growth rate. As a consequence, the unsteady shedding mode II cannot be observed in laboratory experiments. Further, the stationary three-dimensional solution is unstable for Reynolds numbers below the critical value of two-dimensional instabilities. We report for the first time the complete neutral curve as a function of the Reynolds number and rotation rate and identify the absolute critical value of $(Re, \alpha) = (33, 5.8)$. Recent experimental investigations by Linh (2011) confirm the onset of stationary three-dimensional structures at high rotation values with a spanwise periodicity in agreement with our prediction. The structure and the characteristics of the resulting mode, if compared with results obtained using asymptotic theory on inviscid linear flows, suggest that the stationary unstable three-dimensional mode could be the result of a hyperbolic instability.

Acknowledgement

The authors wish to thank D. Fabre for the fruitful discussions on hyperbolic and centrifugal instabilities.

REFERENCES

- BARKLEY, D. & HENDERSON, R. D. 1996 Three-dimensional Floquet stability analysis of the wake of a circular cylinder. *J. Fluid Mech.* **322**, 215–241.
- BARNES, F. H. 2000 Vortex shedding in the wake of a rotating circular cylinder at low Reynolds numbers. *J. Phys. D: Appl. Phys.* **33**, L141–L144.
- CAULFIELD, C. P. & KERSWELL, R. R. 2000 The nonlinear development of three-dimensional disturbances at hyperbolic stagnation points: a model of the braid region in mixing layers. *Phys. Fluids* **12** (5), 1032–1043.
- ELAKOURY, R., BRAZA, M., PERRIN, R., HARRAN, G. & HOARAU, Y. 2008 The three-dimensional transition in the flow around a rotating cylinder. *J. Fluid Mech.* **607**, 1–11.
- FRIEDLANDER, S. & VISHIK, M. M. 1991 Instability criteria for the flow of an inviscid incompressible fluid. *Phys. Rev. Lett.* **66**, 2204–2206.
- GIANNETTI, F. & LUCHINI, P. 2007 Structural sensitivity of the first instability of the cylinder wake. *J. Fluid Mech.* **581**, 167–197.
- KANG, S., CHOI, H. & LEE, S. 1999 Laminar flow past a rotating circular cylinder. *Phys. Fluids* **11** (11), 3321.
- LEBLANC, S. & GODEFERD, F. S. 1999 An illustration of the link between ribs and hyperbolic instability. *Phys. Fluids* **11** (2), 497–499.
- LIFSCHITZ, A. & HAMEIRI, E. 1991 Local stability conditions in fluid dynamics. *Phys. Fluids A* **3** (11), 2644–2651.
- LINH, D.T. T. 2011 Flow past a rotating circular cylinder. PhD thesis, Department of Mechanical Engineering, National University of Singapore.
- LUCHINI, P., GIANNETTI, F. & PRALITS, J. O. 2008 Structural sensitivity of linear and nonlinear global modes. In *Proceedings of 5th AIAA Theoretical Fluid Mechanics Conference, Seattle, Washington, USA*, Paper AIAA-2008-4227.
- MITTAL, S. 2004 Three-dimensional instabilities in flow past a rotating cylinder. *J. Appl. Mech.* **71**, 89–95.

- MITTAL, S. & KUMAR, B. 2003 Flow past a rotating cylinder. *J. Fluid Mech.* **476**, 303–334.
- NOACK, B. R. & ECKELMANN, H. 1994 A global stability analysis of the steady and periodic cylinder wake. *J. Fluid Mech.* **270**, 297–330.
- PRALITS, J. O., BRANDT, L. & GIANNETTI, F. 2010 Instability and sensitivity of the flow around a rotating circular cylinder. *J. Fluid Mech.* **650**, 513–536.
- PROVANSAL, M., MATHIS, C. & BOYER, L. 1987 Bénard–von Kármán instability: transient and forced regimes. *J. Fluid Mech.* **182**, 1–22.
- RAO, A., LEONTINI, J., THOMPSON, M. C. & HOURIGAN, K. 2013 Three-dimensionality in the wake of a rotating cylinder in a uniform flow. *J. Fluid Mech.* **717**, 1–29.
- STOJKOVIĆ, D., BREUER, M. & DURST, F. 2002 Effect of high rotation rates on the laminar flow around a circular cylinder. *Phys. Fluids* **14** (9), 3160–3178.
- STOJKOVIĆ, D., SCHÖN, P., BREUER, M. & DURST, F. 2003 On the new vortex shedding mode past a rotating circular cylinder. *Phys. Fluids* **15** (5), 1257–1260.
- WILLIAMSON, C. H. K. 1996 Vortex dynamics in the cylinder wake. *Annu. Rev. Fluid Mech.* **28**, 477–539.
- YILDIRIM, I., RINDT, C. C. M., VAN STEENHOVEN, A. A., BRANDT, L., PRALITS, J. O. & GIANNETTI, F. 2008 Identification of shedding mode ii behind a rotating cylinder. In *Seventh European Fluid Mechanics Conference, Manchester, UK*. Book of abstracts, p. 371.